CHALMERS
UNIVERSITY OF TECHNOLOGY

Electrochemical investigation of Fe- and Zr-based alloys in standard conditions and under gamma irradiation in contact with H_2O_2

Degree project report in Materials Chemistry

Hannes Nord Nilsson

DEPARTMENT OF CHEMISTRY AND CHEMICAL ENGINEERING

CHALMERS UNIVERSITY OF TECHNOLOGY

Gothenburg, Sweden 2025

www.chalmers.se

Degree project report 2025

Electrochemical investigation of Fe- and Zr-based alloys in standard conditions and under gamma irradiation in contact with H_2O_2

Hannes Nord Nilsson

CHALMERS
UNIVERSITY OF TECHNOLOGY

Department of Chemistry and Chemical Engineering
Chalmers University of Technology
Gothenburg, Sweden 2025

Electrochemical investigation of Fe- and Zr-based alloys in standard conditions and under gamma irradiation in contact with H_2O_2
HANNES NORD NILSSON

Supervisor: Luca Gagliani, Department of Chemistry and Chemical Engineering
Examiner: Christian Ekberg, Department of Chemistry and Chemical Engineering

Degree project report 2025
Department of Chemistry and Chemical Engineering
Chalmers University of Technology
SE-412 96 Gothenburg
Sweden
Telephone +46 31 772 1000

Cover: Image of experimental setup in γ-cell.

Typeset in LaTeX
Gothenburg, Sweden 2025

Electrochemical investigation of Fe- and Zr-based alloys in standard conditions and under gamma irradiation in contact with H_2O_2

HANNES NORD NILSSON
Department of Chemistry and Chemical Engineering
Chalmers University of Technology

Abstract

Radiation induced corrosion is a major problem for the longevity of nuclear power plants, and the research into this field is hampered by the requirement to accurately simulate reactor conditions in experiments. This study attempts to electrochemically investigate the interaction between hydrogen peroxide (H_2O_2) and the alloys AISI 441 and Zircalloy-2 (Zry2), both under standard conditions and under γ irradiation.

The results from the linear scan voltammetry (LSV) indicate that the anodic oxidation reaction between AISI 441 and H_2O_2 might be catalyzed by γ irradiation. Whereas the cathodic reduction reaction may be inhibited by the radiation. With regards to Zry2 the anodic LSV results show a possible surface area limitation on the reaction. The cathodic experiments highlight the chemical inertness that the alloy is known for, though there appears to be a inhibitory effect of γ radiation upon the evolution of hydrogen.

These findings highlight the greater sensitivity of AISI 441 to radioactive environments, which may have implications for material selection in reactor design.

Keywords: Gamma irradiation, Hydrogen peroxide, AISI 441, Zircalloy-2, Electrochemistry

Acknowledgements

I wish to express my gratidude for all the support recieved during this project. I could not have undertaken this project with my supervisor Luca Gagliani, whose patience and guidance has helped me through many struggles. I would also like to extend my thanks to my examiner Christan Ekberg and Ulf Andersson at Nouryon.

Hannes Nord Nilsson, Gothenburg, May 2025

Contents

1
Introduction

Nuclear power as it stands today plays an important part in the plan for transitioning to renewable sources of electricity. The European climate laws state that the European Union should be climate-neutral by 2050 [1]. In order to achieve this goal, fossil fuels need to phased out and renewable sources of electricity need to be phased in. Nuclear power has a relatively low carbon dioxide footprint compared to most other sources of electricity, whether they are renewable or not [2]. This allows nuclear power the unique position of both allowing for the transition to renewable sources of electricity to take place, whilst still having a part in the electricity supply of the future. Whilst nuclear energy offers many advantages in reducing carbon dioxide emissions and in supporting the transition to renewable sources, maintaining the safety and longevity of nuclear power plants remains a concern. One aspect of this involves corrosion in the power plant and understanding the chemical processes that drive this under reactor conditions. One such process is the production, by radiolysis of water, and degradation of hydrogen peroxide (H_2O_2).

The presence of H_2O_2 can have adverse effects in nuclear power plants, including increased corrosion and evolution of hydrogen and oxygen gas. In order to study the effect of H_2O_2 on different structural alloys in an active power plant, the reactor conditions, such as temperature, pressure and irradiation, must be accurately replicated. In this study, the effect of γ-irradiation on the decomposition on H_2O_2 will be studied.

1.1 Background

Previous studies have shown that certain alloys affect the production or consumption of H_2O_2 during γ irradiation, while having little to no effect in the absence of irradiation. This was demonstrated by two experiments, the results of which are shown in figure 1.1: in the first, $4\,cm^2$ alloy samples were immersed in a $0.15\,mM$ H_2O_2 solution ($15\,mL$, $5\,mL$ headspace) for 28 days; in the second, similar samples were placed in pure water and irradiated with $2.2\,MGy$ from a Co^{60} source. In both cases, the H_2O_2 concentration was measured at the end of the exposure.

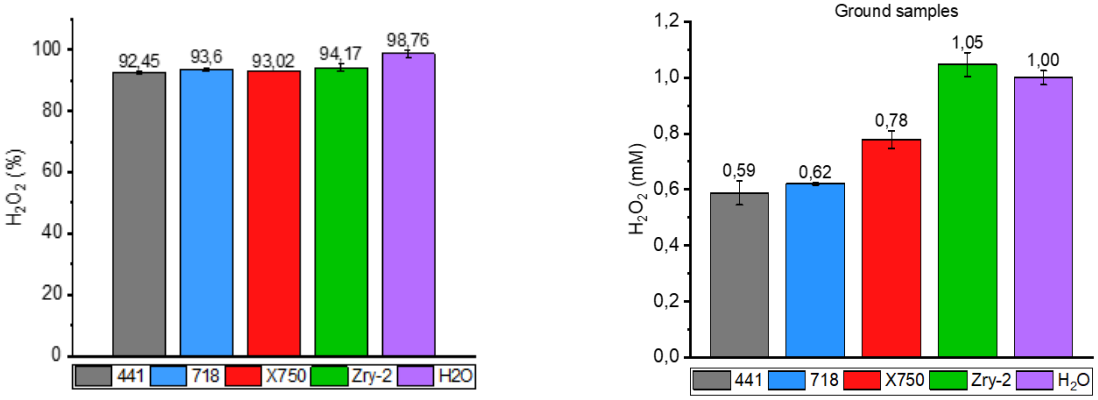

(a) Remaining H_2O_2 in 0.15 mM solution after 28 days.

(b) H_2O_2 after irradiation with 2.2 MGy (normalized to water baseline).

Figure 1.1: Measured H_2O_2 concentrations under two conditions: (a) after 28 days of immersion in 0.15 mM H_2O_2 solution without irradiation, and (b) after irradiation with 2.3 MGy in pure water. The results illustrate the difference in alloy reactivity in the presence and absence of γ-radiation. The data has been adapted from [3].

When designing and constructing nuclear power plants, structural materials are chosen for their durability, corrosion resistance, and tolerance to high temperatures and radiation. These properties are crucial to ensure the reliability and safety of reactors over their operational lifespan. However, the investigation of the properties of the materials is hamstrung by the need to replicate the environment inside an active reactor. Reactor conditions, particularly exposure to intense radiation and the presence of reactive species such as H_2O_2, can significantly accelerate corrosion processes, potentially compromising material performance and posing risks to overall safety. The combination of high radiation levels, elevated temperatures, and chemical interactions in the reactor environment creates a challenging context for material behavior.

Studying the electrochemical behavior of materials under irradiated conditions can provide critical insights into their performance and assist in predicting their long-term integrity. By simulating these harsh conditions in controlled experiments, it can be better understood how materials degrade over time and strategies for mitigating these effects can be identified. By examining the effects of radiation on H_2O_2 and its' interaction with different alloys, a deeper understanding can be reached regarding the mechanism for its' decomposition and how to adequately protect against its effects in the future.

1.2 Purpose

The preliminary aim of this report is to investigate the interaction between H_2O_2 and different alloys under standard and γ-irradiated conditions using an electrochemical cell.

1.3 Goals

The goal of this report is to determine what differences can be observed in the interaction between H_2O_2 and different alloys under standard conditions compared to irradiated conditions.

1.4 Delimitations

The alloys considered will be: AISI 441, and Zircalloy (Zry2). These alloys were chosen since they had, respectively, the largest and smallest effect on the concentration of H_2O_2 in the experiments mentioned above. Additionally, only the effect of γ-radiation from a ^{60}Co-source will be considered.

2

Theory

2.1 Formation and management of H_2O_2 in nuclear reactors

H_2O_2 is generated in nuclear reactors primarily through the radiolysis of water. When liquid water is continuously exposed to ionizing radiation such as γ, it can undergo ionization, producing a water molecular ion (H_2O^+) and a free electron (e^-). The H_2O^+ ion is highly reactive and can in turn interact with another water molecule to produce a hydronium ion (H_3O^+) and a hydroxyl radical ($\cdot OH$). These hydroxyl radicals can subsequently recombine to form hydrogen peroxide as shown in equation 2.1. Figure 2.1 shows the process of radiolysis of water. Over time the concentration of H_2O_2 reaches a steady state where the production rate is in equilibrium with the decomposition, which occurs according to equation 2.2 [4]. Additionally, the H_2O_2 can be decomposed into H_2O and O_2, according to equation 2.3 [5].

$$\cdot OH + \cdot OH \rightarrow H_2O_2 \tag{2.1}$$

$$H_2O_2 + \cdot H \rightarrow H_2O + \cdot OH \tag{2.2}$$

$$2H_2O_2 \rightarrow 2H_2O + O_2^{\uparrow} \tag{2.3}$$

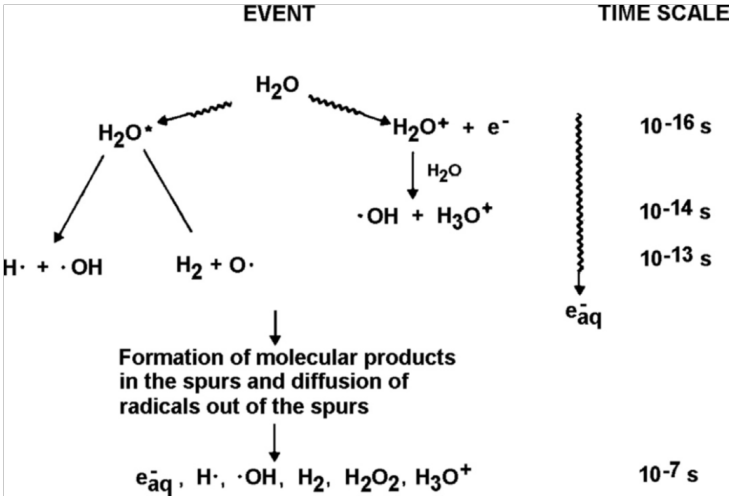

Figure 2.1: Process of radiolysis of water including time scale [6].

The process of radiolysis of water is shown in figure 2.1. The concentration of H_2O_2 in irradiated systems can vary significantly depending on factors such as radiation type, its linear energy transfer (LET)—a measure of energy deposited per unit path length-, dose, chemical environment, and flow conditions. For example, in a research reactor environment, reported concentrations of H_2O_2 range from 0.67 mM to 1.38 mM [7]. There are several measures that are commonly taken in a nuclear reactor to prevent the accumulation of H_2O_2. One such method is the use of hydrogen water chemistry, in which hydrogen gas is injected into the reactor feed water system [8]. In parts of the system with high γ radiation, the hydrogen gas reacts with H_2O_2 to create water according to equation 2.4.

$$H_2 + H_2O_2 \rightarrow 2H_2O \tag{2.4}$$

Additionally the hydrogen can remove O_2 from the system, again by the formation of water [9]. O_2 contributes to the formation of H_2O_2 and to increased corrosion. Depending on the local O_2 concentration in the system, the production of either magnetite or of rust is favored. The corrosion rate for both products is increased by higher O_2 concentrations.

2.2 Catalysis

Catalysis is a process that speeds up chemical reactions without the catalyst itself being consumed in the reaction. Catalysts work by providing an alternative reaction pathway with a lower activation energy, allowing reactants to convert into products more efficiently. They do this by stabilizing intermediate states or bringing reactants together in a way that facilitates bond breaking and forming [10].

There are two main types of catalysis: homogeneous catalysis, where the catalyst is in the same phase as the reactants, and heterogeneous catalysis, where the catalyst exists in a different phase to the reactants, often as a solid interacting with gaseous or liquid reactants[10]. Additionally it must be mentioned that a catalytic effect of a material can be activated by an external phenomena, such a electromagnetic radiation.

2.3 Effect of alloys on H_2O_2 decomposition

ZrO_2 is believed to be catalytic for the surface decomposition of H_2O_2 [11]. However, the effect is believed to be quite weak and leads mostly to the production of O_2, which in turn increases the production rate of H_2O_2.

On the other hand, AISI 441 shows a higher reactivity toward H_2O_2. Previous research has shown that the corrosion rate of stainless steel when exposed to H_2O_2 is related to the Cr content of the steel [12]. AISI 441 has Cr content of 17.5-18.5 % [13], in which range

steels exhibit increased corrosion [12]. A possible reason behind this is that Cr(III) reacts with H_2O_2 forming ·OH radicals [14], which being highly oxidative in turn can increase the corrosion of stainless steels [12].

2.4 Determination of H_2O_2 concentration

H_2O_2 concentration can be measured using UV/Visible spectrometry, a technique that analyzes how a sample absorbs light at specific wavelengths. H_2O_2 by itself has a weak absorbance in the UV/visible range but it can be measured indirectly using a marker with a clear peak in absorbance at a given wavelength. For H_2O_2 commonly I^{3+} in acidic conditions is used and measured at 350 nm.

A key principle governing this measurement is Lambert-Beer's Law (see equation 2.5), which states that absorbance (A) is directly proportional to the concentration (c) of the absorbing species, the path length (l) of the sample cell, and the molar absorptivity (ϵ) of the substance at a given wavelength.

$$A = \epsilon \cdot l \cdot C \tag{2.5}$$

2.5 Electrochemical measurements

There are many types of electrochemical measurements that all serve different purposes. In this section the ones used in this study as well as relevant terminology are briefly explained.

2.5.1 General

In electrochemical experiments, the sample investigated serves as the working electrode (WE). The potential of the WE is either monitored or controlled in relation to a reference electrode (RE), which remains electrochemically stable and does not take part in any reactions. Finally a counter electrode (CE) is used to complete the circuit. Often made out of Pt or graphite, it is chosen to be chemically inert to the system in which it is used. The CE allows for a flow of electrons to or from the WE.

Depending on the the applied potential, oxidation and reduction reactions can take place at the WE or the CE. When the WE has a bias that is more positive (anodic) than the open circuit potential (OCP) of the system, oxidation reactions occur ar its surface, the electrons generated allow for a corresponding reduction reaction to take place on the CE. Vice versa when the WE is biased negatively in relation to the OCP (cathodic), reduction reactions take place on the WE and oxidation on the CE.

The electrons generated during these reactions can be measured as a current, which is related to the rate of the electrochemical reactions taking place. In order for this to occur all three electrodes must be in contact with the electrolyte, a solution that facilitates ionic but not electronic conduction.

2.5.2 Open circuit potential

An OCP measurement is conducted to determine the equilibrium potential of an electrochemical system without the application of an external current [15]. The measured potential is influenced by the electrochemical properties of the WE, the composition and conductivity of the electrolyte, the stability of the RE, and external factors such as temperature, impurities in the electrolyte, and the atmosphere of the system. The OCP value provides important insight into the thermodynamic behavior of the system and is useful for assessing corrosion behavior, reaction kinetics, and material stability under varying environmental conditions.

2.5.3 Chronoamperometry

A chronoamperometry (CA) measurement is used to monitor the current response of an electrochemical system under a fixed applied potential [15]. This response is influenced by the diffusion of electroactive species, the conductivity of the electrolyte, the surface characteristics of the WE, and the stability of the RE.

2.5.4 Cyclic voltammetry

A cyclic voltammetry (CV) measurement is used to study the redox behavior of a system by scanning the potential back and forth between set limits [15]. It is influenced by the scan rate, the diffusion of electroactive species, surface properties of the electrodes, and the conductivity of the electrolyte.

2.5.5 Linear scan voltammetry

A linear scan voltammetry (LSV) measurement is performed to analyze the electrochemical response of a system by applying a potential sweep in one direction at a fixed scan rate [15]. It is affected by the scan rate, mass transport of reactants, electrode surface properties, and solution conductivity. LSV is commonly used to study electrochemical reaction mechanisms, determine onset potentials, and to evaluate catalytic activity in various systems. An LSV can performed in both the anodic and cathodic direction.

3
Methods

3.1 Electrolytic cell

The electrolytic cell used consists of a glass beaker with a electrode holder 3D-printed out of polylatic acid placed on top. A glass beaker was used since a standard electrolytic cell is to a large extent made out of polymers. The change was made to prevent any byproducts from the degradation of said polymers under irradiation in a standard electrolytic cell from affecting the experiment. The electrode holder can be seen in figure 3.1. It was fabricated to maintain the positions of the electrodes relative to each other in order to maintain the repeatability of the experiment. The electrolyte used consisted of Milli-Q water and 1 wt% Na_2SO_4 or alternatively Milli-Q water, 1 wt% Na_2SO_4, and 0.1 mM of H_2O_2. An Ag/AgCl 3 M reference electrode was used and both a platinum and a graphite counter electrode were trialed.

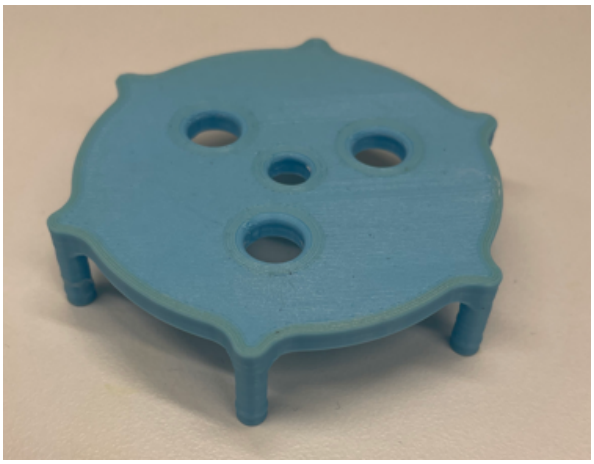

Figure 3.1: 3D-printed electrode holder made out of polylactic acid.

Additionally, various concentrations of H_2O_2 in the electrolyte were trialed. However, since the concentration reached when irradiating Milli-Q water in the γ-cell used stabilized around 0.15 mM, it was decided that using a concentration close to this was optimal as this allowed for the production of our own H_2O_2, which in turn made certain that the electrolyte used was free of any potential contaminants. This concentration also fell within the span observed in a research reactor, as mentioned in chapter 2.

3.2 Sample preparation

The samples were prepared by cutting sheets of the alloys into 3 by 1 cm rectangles and a 2.5 mm hole was drilled through them according to figure 3.2a. The samples were then ground with 500 grit sandpaper. They were then cleaned in an ultrasonic bath with acetone followed by ethanol. The cleaning step is repeated twice to ensure that any contaminants on the surface are removed. The samples are then stored in ethanol until used, a schematic of a sample and a Zry2 sample can be seen in figure 3.2b. Due to material constraints, samples were reused by repeating the grinding and cleaning steps.

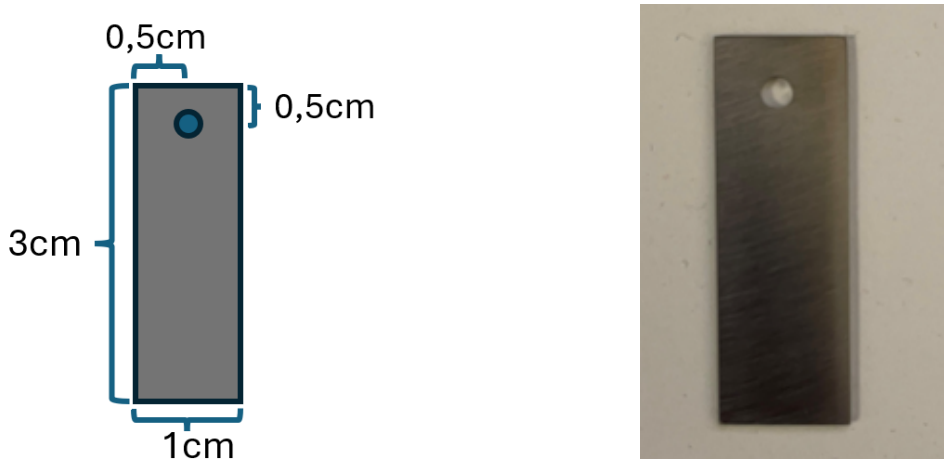

(a) **(b)**

Figure 3.2: a) Schematic of sample. **b)**Image of Zry2-sample after preparation.

3.3 γ-cell

The gamma cell used for this project was a γ-cell 220 from Atomic Energy of Canada Limited with a doserate, determined by Fricke chemical dosimetry, of 48.22 Gy min^{-1} (as of 20-01-2025). The γ-cell can be seen on the title-page. It has an enclosed chamber which is lowered into the base where 12 Co^{60} sources surround the sample, see figure 3.3.

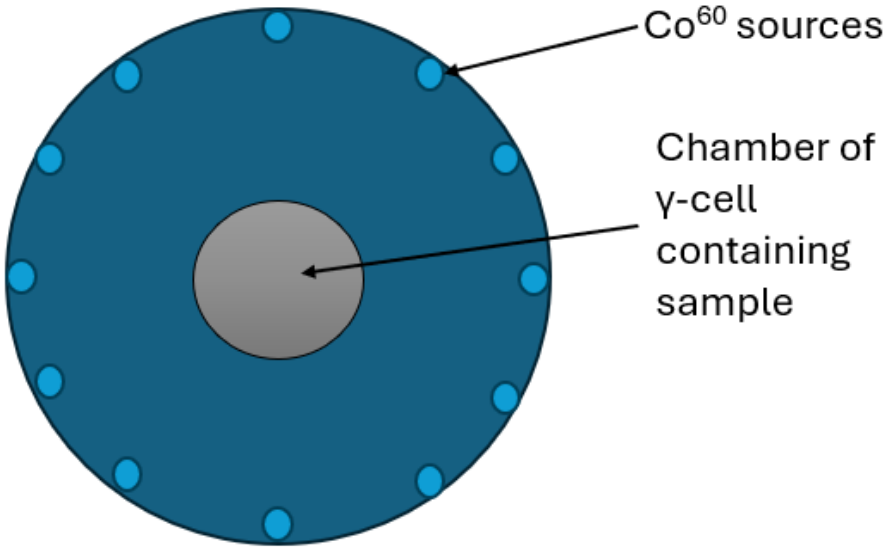

Figure 3.3: Schematic of γ-cell chamber.

3.4 Determination of H_2O_2 concentration using UV/visible light spectrometry

When determining H_2O_2 concentration a VWR UV3000 UV-Vis spectrophotometer was used. To measure the aliquots, 200 μL of 1 M KI solution was mixed with 200 μL of acetate buffer of pH 4.65 doped with ammonium molybdate tetrahydrate and Milli-Q water, 100 μL of sample solution, and 3.6 mL of Milli-Q water. This results in a dilution ratio of 41. A reference is made which contains 100 μL Milli-Q instead of sample. The absorbance from this reference is then subtracted from the absorbance of the sample during calculation. The measurements are performed at 350 nm at which wavelength the molar extinction coefficient is 23.8 L mM^{-1} cm^{-1} [3]. Using equation 2.5 the concentration of H_2O_2 can thus be calculated.

3.5 Counter electrode determination

In order to determine if Pt or graphite was the preferred counter electrode, 3 vials were irradiated with 8.7 kGy of γ radiation. All vials contained 15 mL 0.1 mM H_2O_2 and 1 wt% Na_2SO_4 in milli-Q water and the second and third vials also contained graphite and Pt respectively. After the test was completed, the remaining H_2O_2 concentration was determined. The same test was repeated without γ-radiation.

3.6 Fabrication of an all glass reference electrode

During the development of the methodology used for this project different commercially available Ag/AgCl reference electrodes were trialed. However, since a large number of the parts used in these electrodes were made of resin or polymers, these were proven to fail under repeated irradiation. To ensure repeatability an all glass Ag/AgCl reference electrode was fabricated as shown in figure 3.4.

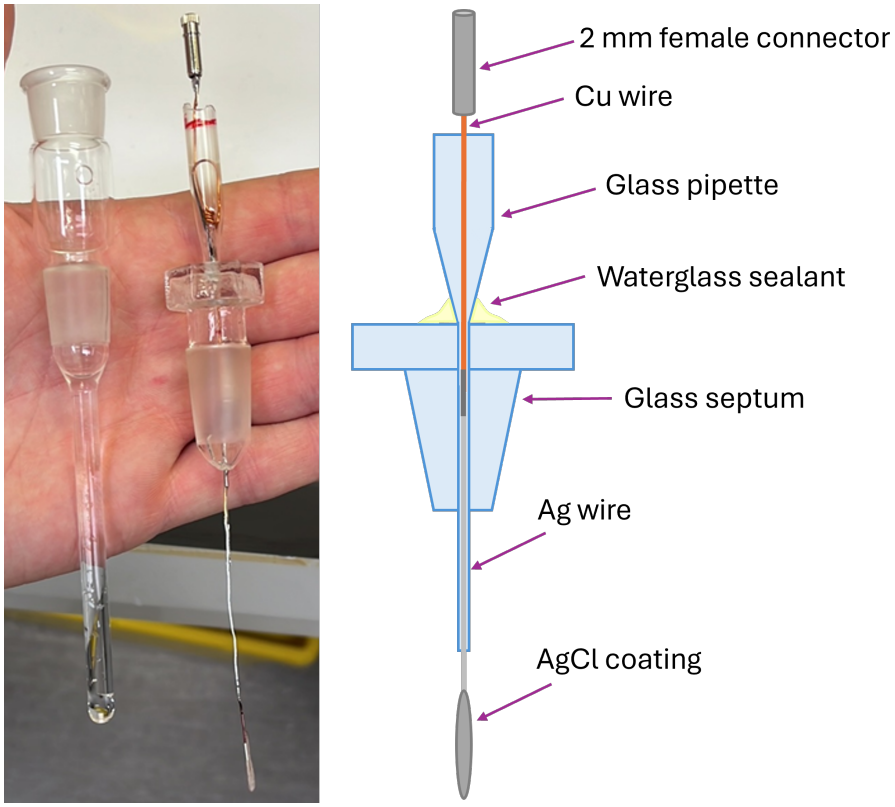

Figure 3.4: A) All glass Ag/AgCl reference electrode split into inner structure and glass bridge. B) Schematic of inner structure [3].

An Ag/AgCl wire was obtained and extended by soldering it to a copper wire. The resulting wire was inserted into a glass Pasteur pipette and then through a glass stopper through which a hole had been drilled. In order to seal the hole a sodium trisilicate (water glass, $(NaOH)_x(Na_2SiO_3)_y \cdot {}_zH_2O$) solution was used at the top. The bottom hole in the stopper was sealed using a blow torch. Finally a female connector was soldered to the top of the copper wire and the core was inserted into a glass bridge. The electrode was filled with 3 M KCl solution and finally tested against a fresh Ag/AgCl electrode, Ag/AgCl, 6.0724.140 from Metrohm, with a maximum difference of 0.3 mV.

3.7 Electrochemical measurements

The samples were hung from a copper wire through the electrode holder, by changing the length of the copper wire the immersion of the sample was controlled, thus exposing 2 by 1 cm of the sample to the electrolyte. The sample is placed facing the reference electrode to ensure that the measured current is not affected by the geometry of the sample. The equipment used was an SP300 potentiostat-galvanostat from BioLogic. The OCP is measured before a constant potential of -0.6 V vs OCP is applied as a means of achieving a clean surface on the WE. The OCP is measured again followed by a CV, from -0.025 V to +0.025 V from the OCP. Finally an anodic LSV, ranging from -0.2 V vs OCP to +1.5 V vs reference electrode with a sweep rate of 1 mV/s is performed. Alternatively a cathodic LSV is performed, ranging from +0.1 V vs OCP to -1.2 V vs reference electrode with a sweep rate of 1 mV/s. The setup as used in the γ-cell can be seen in figure 3.5.

Figure 3.5: The experimental setup in the chamber of the γ-cell.

The experiment is repeated with the same conditions as above in the γ-cell outlined previously to investigate any differences. Additionally the experiment was also performed using a Ar-purged electrolyte.

In order to normalize the variation in current from different samples due to different exposed surface areas, the CV is used. The current amplitude of the CV at the OCP is related to the active area, the scan speed and the potential limits. Since the scan speed

and the potential limits are fixed, the only variable is the active area. By normalizing the current amplitude of the CV to one, and adjusting the current of the LSV by the same factor, the LSVs of the same materials become comparable.

4
Results & Discussion

4.1 Counter electrode determination

The data in table 4.1 illustrate differences in H_2O_2 concentration relative to the amount present without any additives or irradiation. In the absence of irradiation, Pt and graphite both went from 0.1 mM to 0.099 mM, as such there is no significant difference between Pt and graphite. However, under irradiation, graphite led to the smallest reduction in H_2O_2 concentration. The concentration measured was compared to the solution irradiated without Pt or graphite, which went from 0.1 mM to 0.129 mM. Pt and graphite went to 0.117 mM and 0.118 mM respectively. Since the goal was minimizing changes to the system, graphite is the preferred CE.

Table 4.1: Table presenting results determining how much H_2O_2 was consumed by the CE without and during γ irradiation during the same amount of time.

	Absorption	**[H_2O_2] after (mM)**	**Difference vs reference (%)**
Blank	0.046	-	-
Graphite	0.104	0.099	1
Pt	0.107	0.099	1
0.1mM H_2O_2 in γ	0.121	0.129	-
Graphite in γ	0.115	0.118	8.52
Pt in γ	0.114	0.117	9.30

When attempting the experiment with higher concentrations of H_2O_2, insertion of the Pt wire led to rapid bubble formation, believed to be O_2 according to reaction 2.3 even without irradiation, whereas graphite did not visibly react, as can be seen in figure 4.1. This corroborates the result from above.

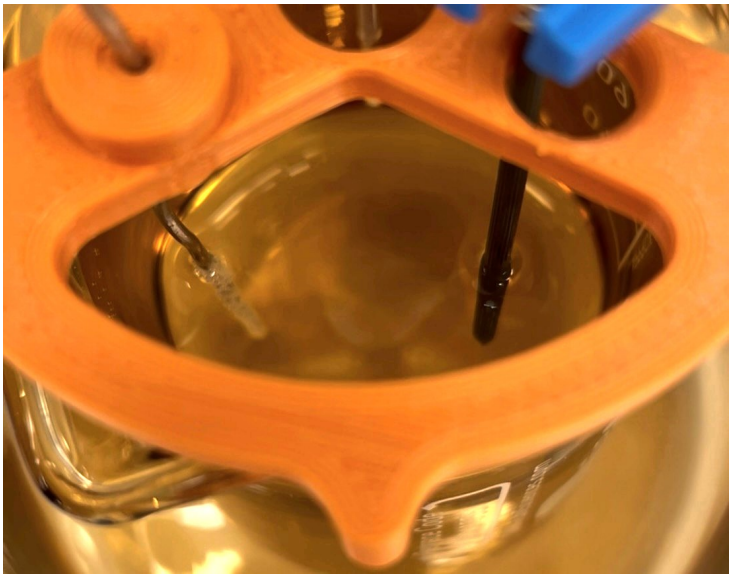

Figure 4.1: Pt (left) & graphite (right) electrode in 0.5 M H_2O_2 solution. Possible O_2 bubbles are visible on Pt.

4.2 Electrochemical investigation under irradiation

To explore the impact of gamma radiation on alloy reactivity, LSVs were carried out on ground samples of AISI 441 and Zry2. Both anodic and cathodic scans were performed to capture potential oxidative and reductive interactions with H_2O_2. Experiments were conducted in air and Ar environments. Argon purging helped isolate the role of oxygen, a key precursor in H_2O_2 production due to radiolysis of water. The anodic LSVs of AISI 441 are shown in figures 4.2 and 4.3.

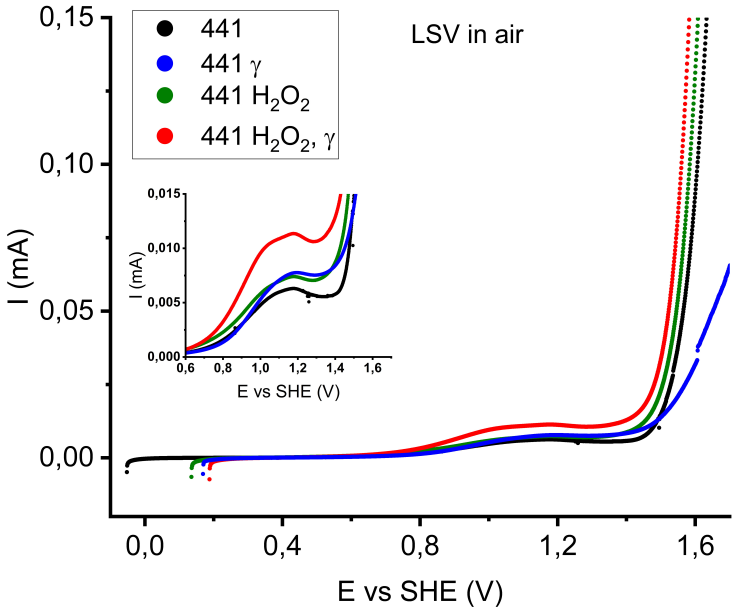

Figure 4.2: Anodic LSV of AISI 441 under non purged conditions. Samples marked with γ have been investigated under irradiated conditions, and the ones marked with H_2O_2 have had 0.1 mM H_2O_2 added to the electrolyte.

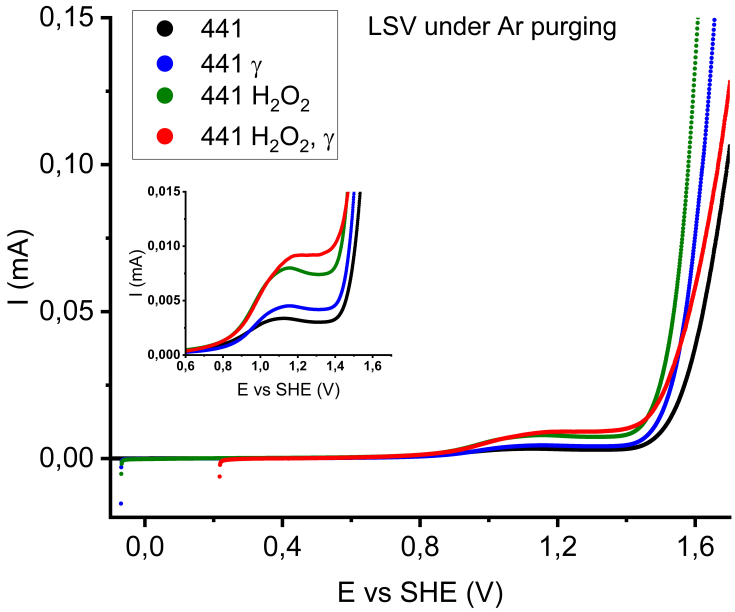

Figure 4.3: Anodic LSV of AISI 441 under Ar-purged conditions. Samples marked with γ have been investigated under irradiated conditions, and the ones marked with H_2O_2 have had 0.1 mM H_2O_2 added to the electrolyte.

In the anodic LSVs visible in figures 4.2 and 4.3, AISI 441 shows different responses depending on the composition of the electrolyte as well as if the sample is irradiated.

These measurements clearly demonstrate the influence of both H_2O_2 and irradiation on the electrochemical behavior of the material. In both purged and non purged conditions, comparing the black and green lines, there is an discernible increase in current from the addition of H_2O_2. Instead comparing the green and the red lines, the γ-irradiation leads to a larger increase, suggesting that the production of additional ·OH from irradiation could contribute to the forced oxidation of a Cr_2O_3 passive layer that is commonly found on stainless steel, the effect of which may be increased by the addition of H_2O_2. Additionally, it may indicate either a catalytic effect upon the interaction or that the production of ·OH by irradiation could increase the conductivity of the system by introducing more charge carriers, thus increasing the current. At 1.5 V there is a sharp increase in current for all samples which is due to the evolution of oxygen gas.

The cathodic LSVs of AISI 441 are visible in figures 4.4 and 4.5.

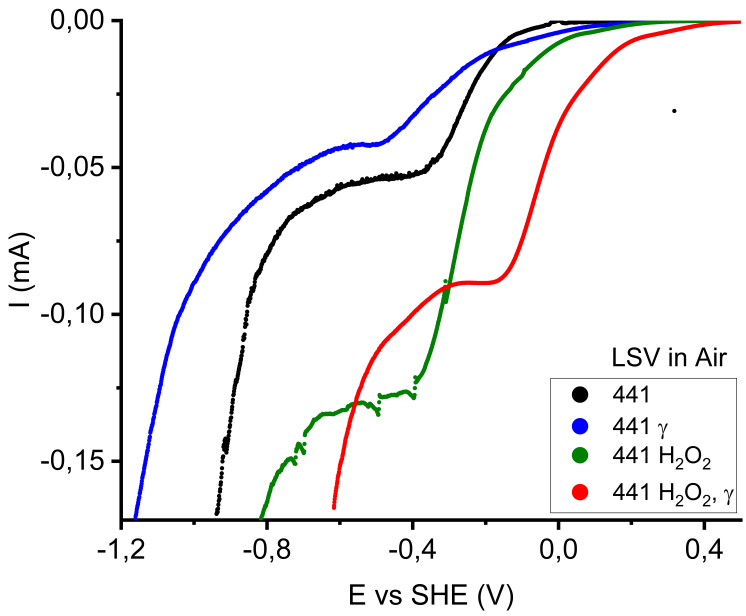

Figure 4.4: Cathodic LSV of AISI 441 under non purged conditions. Samples marked with γ have been investigated under irradiated conditions, and the ones marked with H_2O_2 have had 0.1 mM H_2O_2 added to the electrolyte.

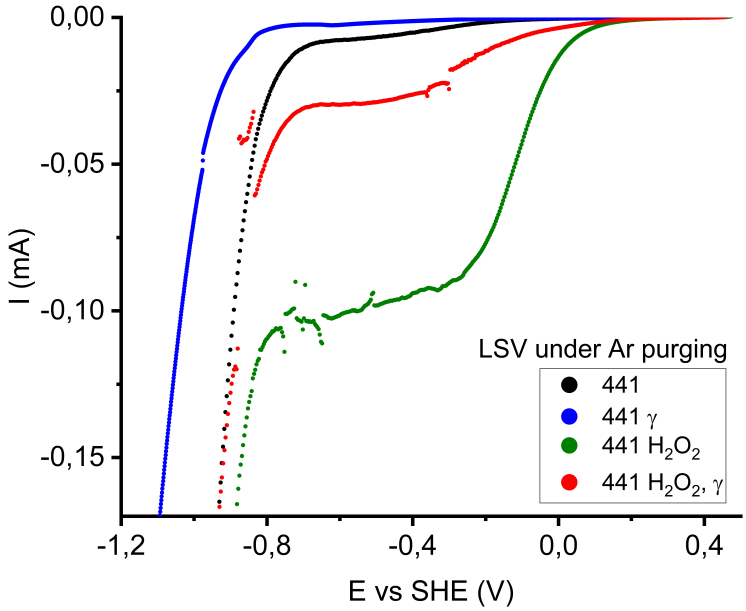

Figure 4.5: Cathodic LSV of AISI 441 under Ar-purged conditions. Samples marked with γ have been investigated under irradiated conditions, and the ones marked with H_2O_2 have had 0.1 mM H_2O_2 added to the electrolyte.

In the cathodic LSVs for AISI 441 shown in figures 4.4 and 4.5, there is a clear difference between the Ar-purged and the non-purged experiments. This difference occurs at around -0.25 V and can be attributed to the contribution from dissolved oxygen. The current under non-purged conditions is consistently higher, confirming oxygen's role as an active electrochemical species. For the experiments without H_2O_2 added, the addition of γ radiation appears to hinder the reaction taking place, resulting in a decreased current (blue line). A possible reason for this is that AISI 441 reduces O_2 around -0.25 V, and that γ radiation instead of catalyzing the reaction, hinders it, thus reducing the current observed. Another reason could be that some oxygen is consumed by the radiolysis of water, and since this decreases the amount of oxygen available to be reduced, the current decreases as well.

During irradiation, when H_2O_2 is added to the electrolyte in the non purged experiments, the plateau is reached at a lower potential (-0.2 V) and at a lower current (-0.1 mA). The potential at which the current increases for the irradiated case (red line) is also less negative than without irradiation (green line), suggesting that the reaction taking place may be catalyzed by the irradiation. The reaction is most likely a combination of oxygen and H_2O_2 reduction.

The purged experiments visible in figure 4.5, in which the contribution from oxygen reduction has been removed, have the same general features. This could indicate that the

reaction taking place from around -0.1 V is the reduction of H_2O_2 (red and green line). However, it is noteworthy that since the current decreases when γ irradiation is applied, one might speculate that the irradiation has an inhibitory effect upon the reduction of H_2O_2. Additionally an important observation is that the evolution of H_2 is delayed by the irradiation of the samples without H_2O_2 added to the electrolyte (black and blue lines). This occurs both in the purged and non purged samples.

The anodic LSVs for Zry2 can be seen in figures 4.6 and 4.7.

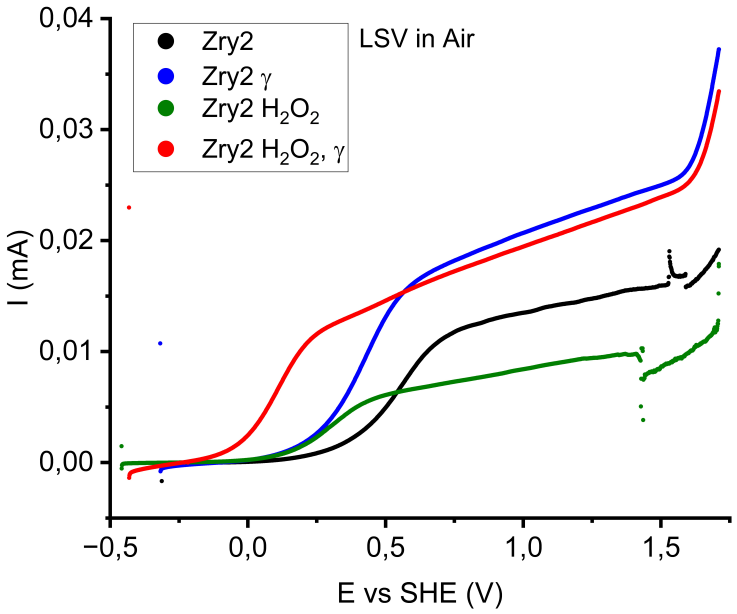

Figure 4.6: Anodic LSV of Zry2-alloy under non purged conditions. Samples marked with γ have been investigated under irradiated conditions, and the ones marked with H_2O_2 have had 0.1 mM H_2O_2 added to the electrolyte.

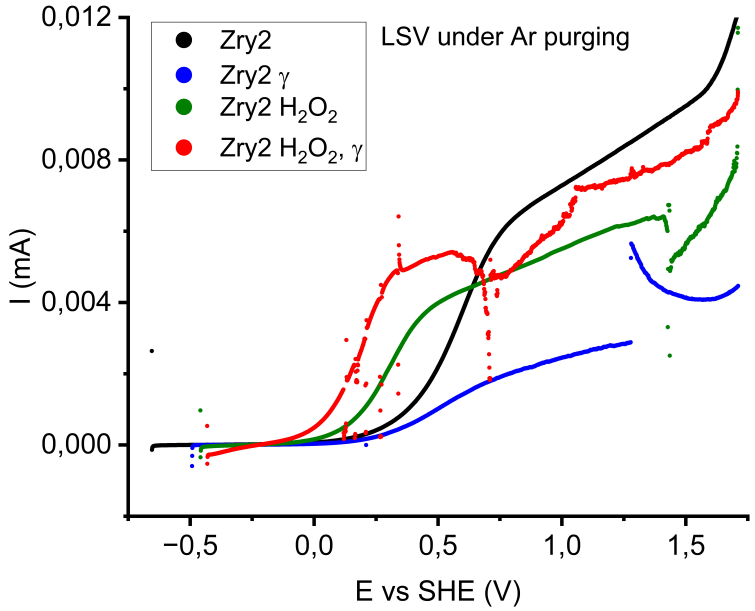

Figure 4.7: Anodic LSV of Zry2-alloy under Ar-purged conditions. Samples marked with γ have been investigated under irradiated conditions, and the ones marked with H_2O_2 have had 0.1 mM H_2O_2 added to the electrolyte.

The anodic LSVs for Zry2 shown in figures 4.6 and 4.7 show quite similar behaviors. Comparing the purged and the non purged experiments, it is clear that the currents are lower without the presence of dissolved oxygen. This indicates that the presence of dissolved oxygen play an influential role in Zry2's reactivity. Interestingly however, in air when irradiated (red and blue line) the current reaches about the same level. This could indicated that the reaction is surface area limited which can lead to a breakdown of the passivation layer and localized corrosion.
In both purged and non purged conditions, the onset potential for the reaction taking place is reduced by the addition of H_2O_2 (green line). When purging without H_2O_2 however, there is an decrease in current when irradiated (blue line). Irradiation with H_2O_2 added results in a larger increase in current (red line). Additionally the current under Ar-purged conditions is much lower than when oxygen is present. This reinforces the conclusion that dissolved oxygen is a key electroactive species in this system.
The LSVs all have generally the same shape with an increase in current starting from -0.25 V to 0.75 V at which point the gradient is much reduced. Around 1.5 V there is a large increase in current due to the evolution of oxygen gas. The purged experiments suffered from disturbances to the system from external factors. In order to draw any clear conclusions from these, the experiments would have to be repeated. Potential sources of error include vibrations from external sources and formation of bubbles on electrode surfaces.

The final experiments were the cathodic LSVs of Zry2, the results of which are shown in figures 4.8 and 4.9.

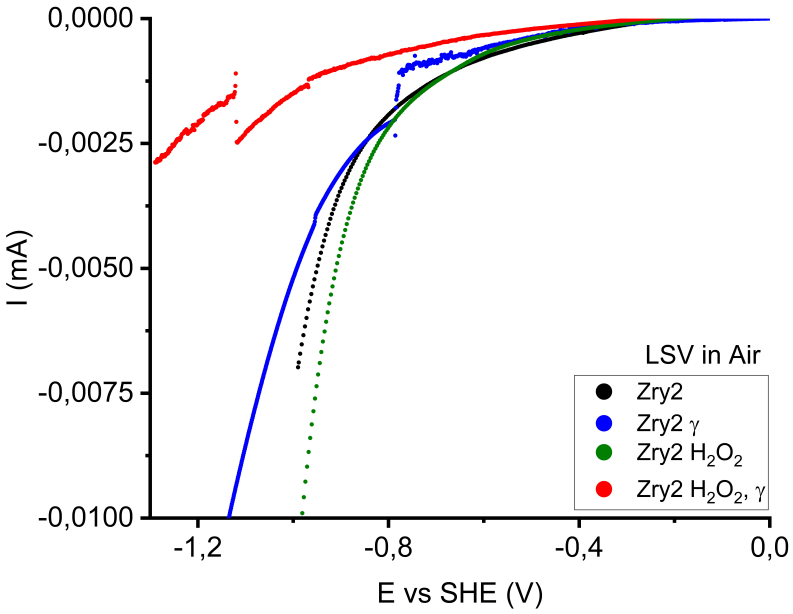

Figure 4.8: Cathodic LSV of Zry2-alloy under non purged conditions. Samples marked with γ have been investigated under irradiated conditions, and the ones marked with H_2O_2 have had 0.1 mM H_2O_2 added to the electrolyte.

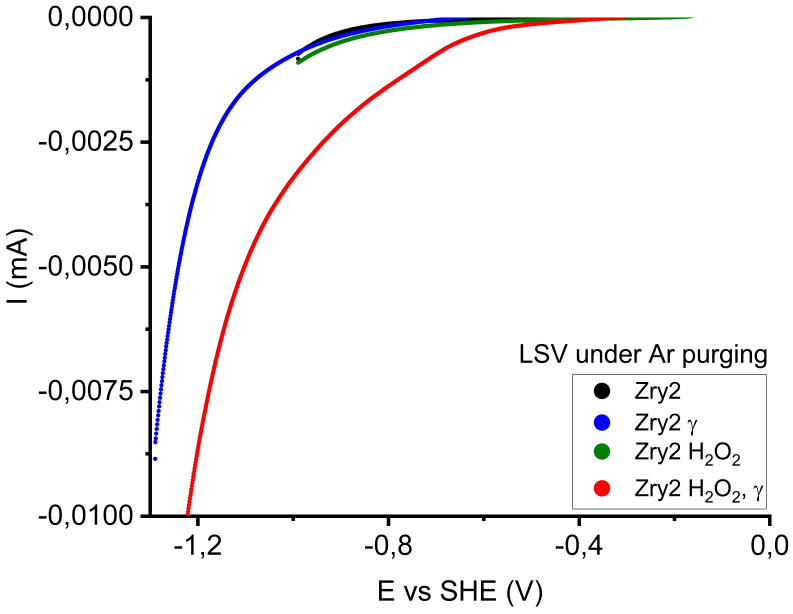

Figure 4.9: Cathodic LSV of Zry2-alloy under Ar-purged conditions. Samples marked with γ have been investigated under irradiated conditions, and the ones marked with H_2O_2 have had 0.1 mM H_2O_2 added to the electrolyte.

The cathodic LSVs of Zry2 visible in figures 4.8 and 4.9 highlight the lack of reactivity that is associated with Zry2-alloys. The experiments all have generally the same features regardless of conditions. Around -0.8 V hydrogen evolution is visible as a large increase in current. This behavior is consistent across all conditions tested, reaffirming Zry2's general electrochemical inertness within the investigated potential window. Interestingly, in non purged experiments the addition of H_2O_2 and irradiation appears to decrease the rate of increase of the H_2 evolution, whilst under Ar-purged conditions the H_2 evolution occurs more rapidly. Unfortunately some of the experiments were halted early due to external influences, limiting the conclusions that can be drawn from this data. However, it must be noted that the onset potential for the H_2 evolution remains consistent throughout the experiments.
The AISI 441 samples show an increased reactivity with H_2O_2 under γ radiation, as evidenced by a peak in current around 1.2 V in the anodic LSV as seen in figure 4.3 and by a inhibitive effect resulting in a reduction in current around -0.4 V for the cathodic LSV in figure 4.5. This suggests an active electrochemical interaction between the alloy and H_2O_2. The increased current on the anodic side and reduced current on the cathodic side is visible under both Ar-purged and non purged conditions. Therefore, γ irradiation may catalyze not only the reaction with H_2O_2 but also with dissolved oxygen. This dual effect could imply a broader sensitivity of AISI 441 to irradiated environments, potentially making it a more reactive or corrosion-prone material in irradiated aqueous systems. This result is in agreement with the experiments performed prior to this thesis as mentioned in section 1.1.

It is noteworthy that the Zry2 samples all have lower currents than their AISI 441 counterparts, revealing that Zry2 has a lower reactivity to both oxygen and H_2O_2. This consistent difference supports the conclusion that Zry2 exhibits inherently lower electrochemical activity. However, as all Zry2 samples are normalized relative to each other and AISI 441 to the other AISI 441 samples they are not directly comparable. Therefore, only general trends can be inferred when comparing the two materials. Future work should consider cross-normalization techniques to facilitate more accurate material-to-material comparisons.

5
Conclusion

5.1 Summary of findings

The electrochemical studies performed during this project indicate an increased reactivity of AISI 441 to H_2O_2 under γ irradiation. Additionally, the cathodic experiments on AISI 441 show a possible inhibitory effect of γ radiation upon the reaction with H_2O_2.
The anodic experiments performed on Zry2 under γ irradiation show a possible surface area limitation in the reaction in non purged conditions. Whilst the cathodic experiments highlight the low reactivity that Zry2 is known for, there appears to be a inhibitory effect of γ radiation upon the evolution of hydrogen.

5.2 Suggestions for improvements in further studies

Future work should consider cross-normalization techniques to allow for more accurate material-to-material comparisons. This could be done by adding a precise amount of electrolyte to the electrochemical cell, by ensuring that the hole used for hanging the samples was placed consistently, and by increasing the control over the shape of the samples by using samples that had only been ground once in the experiments. Applying these measures would allow for greater comparisons between the materials. Additionally, in order to improve the reliability of the measurements, they should be performed in a Faraday cage, repeated in triplicate and continued until clear evidence of hydrogen or oxygen evolution takes place to ensure consistency.

Bibliography

[1] *Renewable energy*, eng, Nov. 2024. [Online]. Available: https://www.eea.europa.eu/en/topics/in-depth/renewable-energy (visited on 05/05/2025).

[2] *Nuclear essentials - world nuclear association*. [Online]. Available: https://world-nuclear.org/nuclear-essentials/how-can-nuclear-combat-climate-change (visited on 05/05/2025).

[3] L. Gagliani, *Effects of gamma radiation on water chemistry, polymers and fe-, ni- and zr-based alloys*, eng, Thesis for the degree of licentiate of engineering at Chalmers University of Technology, 2025.

[4] A. O. Allen, "Radiation chemistry of aqueous solutions", eng, *The Journal of Physical and Colloid Chemistry*, vol. 52, no. 3, pp. 479–490, Mar. 1948, ISSN: 0092-7023, 1541-5740. DOI: 10.1021/j150459a009. [Online]. Available: https://pubs.acs.org/doi/abs/10.1021/j150459a009 (visited on 05/02/2025).

[5] E. Erasmus, J. O. Claassen, and W. A. van der Westhuizen, "Catalytic wet peroxide oxidation of formic acid in wastewater with naturally-occurring iron ore", en, *Water SA*, vol. 42, no. 3, pp. 442–448, Jul. 2016, ISSN: 1816-7950. DOI: 10.4314/wsa.v42i3.09. [Online]. Available: http://www.scielo.org.za/scielo.php?script=sci_abstract&pid=S1816-79502016000300009&lng=en&nrm=iso&tlng=en (visited on 05/05/2025).

[6] G. R. Choppin, J.-O. Liljenzin, J. Rydberg, and C. Ekberg, *Radiochemistry and nuclear chemistry*, eng, 4th edition. Amsterdam Boston: Elsevier/AP, Academic Press is an imprint of Elsevier, 2013, ISBN: 9780124058972.

[7] C. C. Chan, P. C. Liu, and P. S. Weng, "Determination of hydrogen peroxide concentration in THOR coolant during reactor operation", eng, *Journal of Radioanalytical and Nuclear Chemistry Letters*, vol. 87, no. 4, pp. 267–272, Oct. 1984, ISSN: 0236-5731, 1588-2780. DOI: 10.1007/BF02167431. [Online]. Available: http://link.springer.com/10.1007/BF02167431 (visited on 01/28/2025).

[8] U.S. Nuclear Regulatory Commission, *Boiling water reactor vessel and internals project: Technical basis for hydrogen water chemistry and noble metal chemical addition*, eng, NUREG/CR-6907, 2021. [Online]. Available: https://www.nrc.gov/docs/ML2128/ML21286A518.pdf (visited on 04/29/2025).

[9] CED Engineering, *Reactor water chemistry*, eng, Course H03-001, n.d. [Online]. Available: https://www.cedengineering.com/userfiles/H03-001%20-%20Reactor%20Water%20Chemistry%20-%20US.pdf (visited on 04/29/2025).

[10] P. W. Atkins and J. de Paula, *Atkins' physical chemistry*, eng, Tenth edition. Oxford: Oxford University Press, 2014, pp. 840, 955, ISBN: 9780199697403.

[11] N. G. Petrik, A. B. Alexandrov, and A. I. Vall, "Interfacial energy transfer during gamma radiolysis of water on the surface of zro_2 and some other oxides", eng, *The Journal of Physical Chemistry B*, vol. 105, no. 25, pp. 5935–5944, Jun. 2001,

ISSN: 1520-6106, 1520-5207. DOI: 10.1021/jp004440o. [Online]. Available: https://pubs.acs.org/doi/10.1021/jp004440o (visited on 04/08/2025).

[12] A. Ubaldini, C. Telloli, A. Rizzo, *et al.*, "A study of accelerated corrosion of stainless steels under highly oxidizing conditions", eng, *Coatings*, vol. 14, no. 4, p. 390, Mar. 2024, ISSN: 2079-6412. DOI: 10.3390/coatings14040390. [Online]. Available: https://www.mdpi.com/2079-6412/14/4/390 (visited on 04/29/2025).

[13] A. Unterstell, *1. 4509(AISI 441) , s43940 | datasheet | metalcor*, eng. [Online]. Available: https://www.metalcor.de/en/datenblatt/25/ (visited on 04/29/2025).

[14] T.-C. Tsou and J.-L. Yang, "Formation of reactive oxygen species and DNA strand breakage during interaction of chromium(Iii) and hydrogen peroxide in vitro: Evidence for a chromium(Iii)-mediated Fenton-like reaction", eng, *Chemico-Biological Interactions*, vol. 102, no. 3, pp. 133–153, Dec. 1996, ISSN: 00092797. DOI: 10.1016/S0009-2797(96)03740-4. [Online]. Available: https://linkinghub.elsevier.com/retrieve/pii/S0009279796037404 (visited on 04/29/2025).

[15] L. L. Faulkner and A. J. Bard, *Electrochemical methods and applications*, eng, 2nd ed. New Yor: Wiley, 2001, pp. 5, 158, 227, ISBN: 9780471043720.

DEPARTMENT OF CHEMISTRY AND CHEMICAL ENGINEERING
CHALMERS UNIVERSITY OF TECHNOLOGY
Gothenburg, Sweden
www.chalmers.se

CHALMERS
UNIVERSITY OF TECHNOLOGY